Biology of Reproduction, 2022, **106(5)**, 1000–1010
https://doi.org/10.1093/biolre/ioac015
Advance access publication date 9 February 2022
Research Article

Irx3 promotes gap junction communication between uterine stromal cells to regulate vascularization during embryo implantation†

Ryan M. Brown[1], Linda Wang[1], Anqi Fu[1], Athilakshmi Kannan[2], Michael Mussar[1], Indrani C. Bagchi[2,*] and Joan S. Jorgensen[1,*]

[1]Department of Comparative Biosciences, University of Wisconsin-Madison, Madison, WI, USA
[2]Department of Comparative Biosciences, University of Illinois at Urbana Champaign, Urbana, IL, USA

***Correspondence:** Department of Comparative Biosciences, University of Illinois at Urbana Champaign, Urbana, IL, USA. E-mail: ibagchi@illinois.edu (Indrani Bagchi); Department of Comparative Biosciences, University of Wisconsin-Madison, Madison, WI, USA. E-mail: joan.jorgensen@wisc.edu (Joan S. Jorgensen)

†**Grant Support:** National Institutes of Health, Eunice Kennedy Shriver National Institute Of Child Health & Human Development (NIH-NICHD) R01HD075079 (JSJ). National Institutes of Health, Eunice Kennedy Shriver National Institute Of Child Health & Human Development (NIH-NICHD) R01HD090066 (IB). Endocrinology and Reproductive Physiology Training Grant, and National Institutes of Health (NIH-NICHD) T32HD41921 (AF).

Abstract

Appropriate embryo-uterine interactions are essential for implantation. Besides oocyte abnormalities, implantation failure is a major contributor to early pregnancy loss. Previously, we demonstrated that two members of the Iroquois homeobox transcription factor family, IRX3 and IRX5, exhibited distinct and dynamic expression profiles in the developing ovary to promote oocyte and follicle survival. Elimination of each gene independently caused subfertility, but with different breeding pattern outcomes. *Irx3* KO (*Irx3*$^{LacZ/LacZ}$) females produced fewer pups throughout their reproductive lifespan which could only be partially explained by poor oocyte quality. Thus, we hypothesized that IRX3 is also expressed in the uterus where it acts to support pregnancy. To test this hypothesis, we harvested pregnant uteri from control and *Irx3* KO females to evaluate IRX3 expression profiles and the integrity of embryo implantation sites. Our results indicate that IRX3 is expressed in the endometrial stromal cells at day 4 of pregnancy (D4) with peak expression at D5–D6, and then greatly diminishes by D7. Further, studies showed that while embryos were able to attach to the uterus, implantation sites in *Irx3* KO pregnant mice exhibited impaired vascularization and abnormal expression of decidualization markers. Finally, we also observed an impaired response of the *Irx3* KO uteri to an artificial deciduogenic stimulus, indicating a critical role of this factor in regulating the decidualization program. Together, these data established that IRX3 promotes female fertility via at least two different mechanisms: (1) promoting competent oocytes and (2) facilitating functional embryo–uterine interactions during implantation.

Summary Sentence

Irx3 promotes successful embryo-uterine interactions in mice.

Keywords: Uterus, Decidualization, Angiogenesis, Pregnancy, Fertility, Iroquois

Introduction

Embryo implantation is achieved when a competent oocyte is fertilized and then develops into a blastocyst capable of facilitating embryo–uterine interactions with the receptive endometrium. In humans, it has been reported that approximately two thirds of pregnancies are lost due to implantation failure. Uncovering the signaling pathways and downstream mediators that govern implantation is necessary to improve outcomes associated with defective embryo implantation including ectopic pregnancies, implantation failure and infertility (reviewed in [1]).

In the mammalian uterus, steroid hormones estrogen and progesterone induce structural and functional changes during early pregnancy to support embryo implantation [2–5]. Of these changes, uterine stromal differentiation, or decidualization, is a critical response to embryo recognition that initiates extensive tissue remodeling for proper maternal–fetal interactions during early pregnancy. During decidualization, the endometrial stromal cells of the uterus undergo differentiation into decidual cells with unique biosynthetic and secretory profiles needed to promote tissue transformation and uterine vascular remodeling [6–8]. In the murine model, implantation begins on day (D) 4 midnight, with the majority of decidualization occurring between D5 and D8, and establishment of pregnancy by D10–D11 of gestation [9]. Complementary timing occurs in the human uterus where, for a short window of time, during the mid-secretory phase of each menstrual cycle, the uterus becomes "receptive" to embryo implantation and the decidualization process begins [10]. In both the mouse and human, decidualization promotes tissue remodeling and neovascularization, which are critical events for successful establishment of pregnancy. A major challenge is deciphering the signaling mechanisms governing successful maternal–fetal interactions during early pregnancy. To this end, it is necessary to identify and characterize factors that regulate decidualization and angiogenesis during embryo implantation.

The Iroquois factors are highly conserved proteins that have been implicated in patterning and embryogenesis in animal kingdoms spanning invertebrate to vertebrate. In mammals, there are a total of six Iroquois genes clustered in two

Received: May 10, 2021. **Revised:** November 16, 2021. **Accepted:** February 7, 2022

groups, with cluster A (*Irx1,2,4*) and cluster B (*Irx3,5,6*) located on chromosomes 5 and 16 in the human and chromosomes 8 and 13 in the mouse, respectively [11, 12]. Previously, we discovered that null mutation of both *Irx3* and *Irx5* resulted in abnormal granulosa cell morphology and disrupted granulosa cell–oocyte interactions [13]. A closer look, using $Irx3^{LacZ/LacZ}$ single knockout mice, revealed that although mutant females could become pregnant, loss of *Irx3* caused a decrease in birthrate to approximately half as many pups compared to controls throughout a 6-month breeding study. While $Irx3^{LacZ/LacZ}$ females demonstrated abnormalities in follicle survival, this did not fully explain the subfertility phenotype [13].

Although evidence points to an oocyte deficit with loss of *Irx3*, relatively normal ovarian histology led us to hypothesize that another facet in the female reproductive axis could also be disrupted. Due to the decrease in pup accumulation over time, we hypothesized that embryo implantation was compromised due to loss of *Irx3*. Evaluation of implantation sites within $Irx3^{LacZ/LacZ}$ pregnant females demonstrated impaired vascularization and a significant reduction in pups by D7 of pregnancy. Herein, we report for the first time that *Irx3* is expressed in the mouse uterus overlapping the window of implantation when it plays a critical role in neoangiogenesis. Our results suggest disruptions are caused by unorganized gap junction (GJA1) protein expression. Together, these findings reveal the multifaceted role of *Irx3* in female fertility.

Materials and methods

Ethics statement

Animals were euthanized by CO_2 asphyxiation followed by cervical dislocation. Animal housing and all described procedures were reviewed and approved by the Institutional Animal Care and Use Committee at the University of Wisconsin—Madison and were performed in accordance with the National Institute of Health Guiding Principles for the Care and Use of Laboratory Animals.

Animals

Mice were housed in disposable, ventilated cages (Innovive, San Diego, CA). Rooms were maintained at 22 ± 2°C and 30–70% humidity on a 12-h light/dark cycle. Mouse strains included CD1 outbred mice (Crl:CD1(ICR), Charles River, Wilmington, MA, USA) and $Irx3^{LacZ}$ [14], all of which were maintained on a CD1 genetic background. Genotyping was carried out as previously reported [13, 14]. Pregnancies were the result of breeding between CD1 (wild type (WT) control) or $Irx3^{LacZ/LacZ}$ females and CD1 males. Thus, all embryos generated in $Irx3^{LacZ/LacZ}$ females were $Irx3^{+/LacZ}$. Timed mating was identified as the presence of a vaginal plug after mating which was designated as day 1 (D1) of pregnancy.

Tissue processing and histology

Uterine tissue was harvested at the indicated time points, fixed in 10% neutral buffer formalin (NBF) in phosphate-buffered saline (PBS) at 4°C overnight. Uteri were collected on D7 of gestation, dehydrated through an ethanol gradient, cleared in xylene and embedded in paraffin. Paraffin blocks were sectioned at 5 μm thickness, mounted on slides and then stained with hematoxylin and eosin (H&E) for histological analysis.

Artificial decidualization

Uterine stromal cell decidualization was experimentally induced in adult non-pregnant, hormone-primed mice as described previously [15]. Briefly, $Irx3^{LacZ/LacZ}$ and litter mate control female mice were ovariectomized to remove any circulating hormones. Two weeks following ovariectomy, animals were injected with 100 ng of E_2 in 0.1 mL of corn oil subcutaneously (sc) every 24 h for three consecutive days. After two days of rest, sc hormone injections were given daily, containing 1 mg P_4 and 10 ng E_2 in 0.1 mL for three consecutive days. Decidualization was initiated in one horn by injecting 50 μL of oil into the lumen, while the other horn was left unstimulated. Mice were treated with additional $E_2 + P_4$ for up to 48 h post-stimulus. Mice were euthanized and uterine horns were collected.

Alkaline phosphatase staining

Frozen uterine sections were fixed in 10% NBF for 10 min, and then washed with 1x PBS three times for 5 min each. The uterine sections were then incubated in the dark at 37°C for 30 min in a solution containing 0.5 mM naphthol AS-MX phosphate (ALPL substrate) and 1.5 mM Fast Blue RR in 0.1 M Tris–HCl, pH 8.5. Alkaline phosphatase activity releases orthophosphate and naphthol derivatives from the ALPL substrate. The naphthol derivatives are simultaneously coupled with the diazonium salt to form a dark dye marking the site of enzyme action. The slides were rinsed in tap water to terminate the enzymatic reaction. Stained uterine sections were visualized under an Olympus BX51 microscope.

Immunohistochemistry/immunofluorescence

Uterus tissue sections were deparaffinized in xylene, rehydrated through a series of ethanol washes, and then rinsed in water. Antigen retrieval was performed by immersing the slides in 0.1 M citrate buffer solution at pH 6.0 or EDTA buffer at pH 8 depending on antibody specifications (Supplementary Table S1), and heated in a water bath at 80°C for 25 min. The slides were allowed to cool, rinsed in water, followed by PBS washes. The slides were then incubated at room temperature with 10% donkey solution for 1 h before incubating them with primary antibody overnight at 4°C. The following morning, tissues were washed in PBS before incubating with secondary antibody for 1 h, then washed with PBS, incubated with a 10X DAPI (4′,6-diamidino-2-phenylindole) in PBS solution (1:500) as a nuclear counterstain for 10 min, followed by 3 min with Vector True View Kit (Vector Laboratories, SP-8400, Burlingame, CA), and mounted. Immunofluorescence was repeated in uterine sections collected from at least three animals. Quantification of IHC was performed using Image J, the mean fluorescence intensity of CD31 ($n = 3$ for each group) or GJA1 ($n = 3$–4 for each group) was quantified using the ROI manager on both the mesometrial and anti-mesometrial regions surrounding the embryo. Images were collected on a Leica SP8 confocal microscope for IHC and a Keyence BZ-X700 microscope for H&E.

Quantitative real-time polymerase chain reaction analysis

Uterine tissue was homogenized, and total RNA was extracted using TRIZOL reagent (Invitrogen, 15596026, Waltham, MA, USA), according to the manufacturer's protocol and quantified using a NanoDrop 2000. Around 500 ng from each sample was used for first-strand complementary DNA syn-

Table 1. List of primers used

Gene	Forward primer	Reverse primer
36b4	5′-CGACCTGGAAGTCCAACTAC-3′	5′-ATCTGCTGCATCTGCTTG-3′
Irx3	5′-CGCCTCAAGAAGGAGAACAAGA-3′	5′-CGCTCGCTCCCATAAGCAT-3′
Hand2	5′-AGAAAACAGGGCCGCTAACA-3′	5′-TCTCCTCTTTCACGTCGGTC-3′
Esr1	5′-GCCAAGGAGACTOGCTACTG-3′	5′-CTCCCGGTTCTTGTCAATGGT-3′
Pgr	5′-CTAAATGAGCAGAGGATGAAGGAG-3′	5′-TGGGCAACTGGGCAGCAATAAC-3′
Wnt4	5′-TTCTCACAGTCCTTTGTGGACG-3′	5′-TCTGTATGTGGCTTGAACTGTG-3′
Cebpb	5′-AGCGACGAGTACAAGATG-3′	5′-CTGCTCCACCTTCTTCTG-3′
Prl8a2/Prp	5′-CTCACTTCTCAGGGGCACTC-3′	5′-GGATCTGAGCAGCCATTCTC-3′
Gja1	5′-CTATCGTGGATCAGCGACCTTC-3′	5′-CACGGGAACGAAATGAACACC-3′

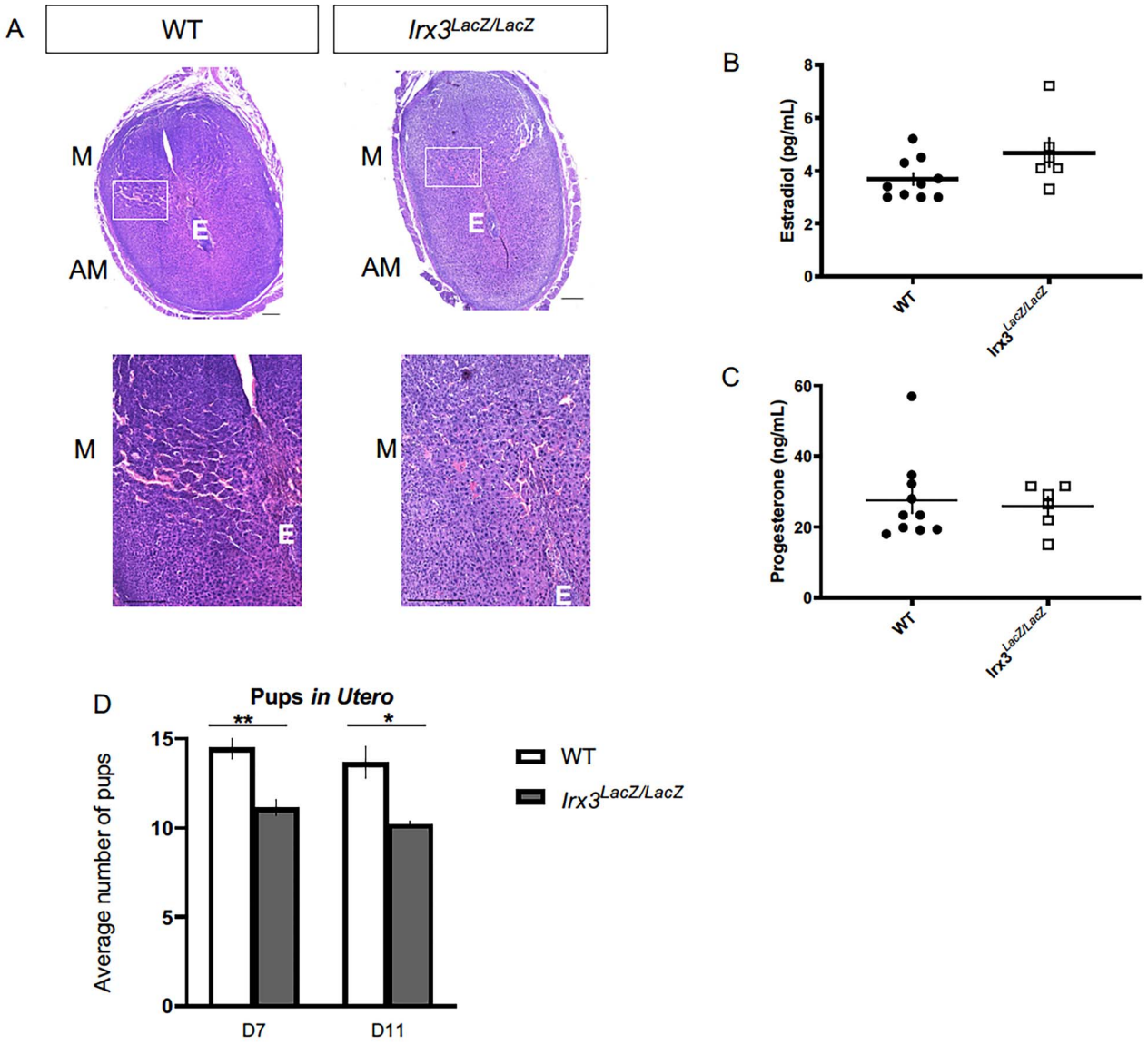

Figure 1. *Irx3*$^{LacZ/LacZ}$ causes deficits in uterine vascularization and subfertility. (A) H&E staining of D7 wild type (WT, $n=6$) and *Irx3*$^{LacZ/LacZ}$ ($n=6$) pregnant uteri. Scale bars, 250 mm. The white boxes are enlarged in the images below each section. AM: anti-mesometrial; M: mesometrial; E: embryo. (B, C) Circulating estradiol (B) and progesterone (C) were measured at D7 of gestation (WT, $n=10$; *Irx3*$^{LacZ/LacZ}$, $n=6$). (D) Average number of implantation sites *in utero* at D7 (WT $n=8$; *Irx3*$^{LacZ/LacZ}$ $n=7$) and D11 (WT $n=3$; *Irx3*$^{LacZ/LacZ}$ $n=5$). Data in D represent the mean ± SEM. Statistics: two-sample *t*-test, *: $P<0.05$; **: $P<0.01$.

thesis by SuperScriptII (Invitrogen, AM9515, Waltham, MA, USA). Complementary DNA was diluted 1:5 and then 2 μL was added to 5 μL SYBR green polymerase chain reaction (PCR) mixture (BioRad, 1725271, Hercules, CA, USA), 2.4 μL water and 1.25 pmol primer mix. PCRs were carried out using the BioRad CFX96 system and RNA transcripts were quantified using the $\Delta\Delta$Ct method (Livak & Schmittgen, 2001). Primers are shown in Table 1.

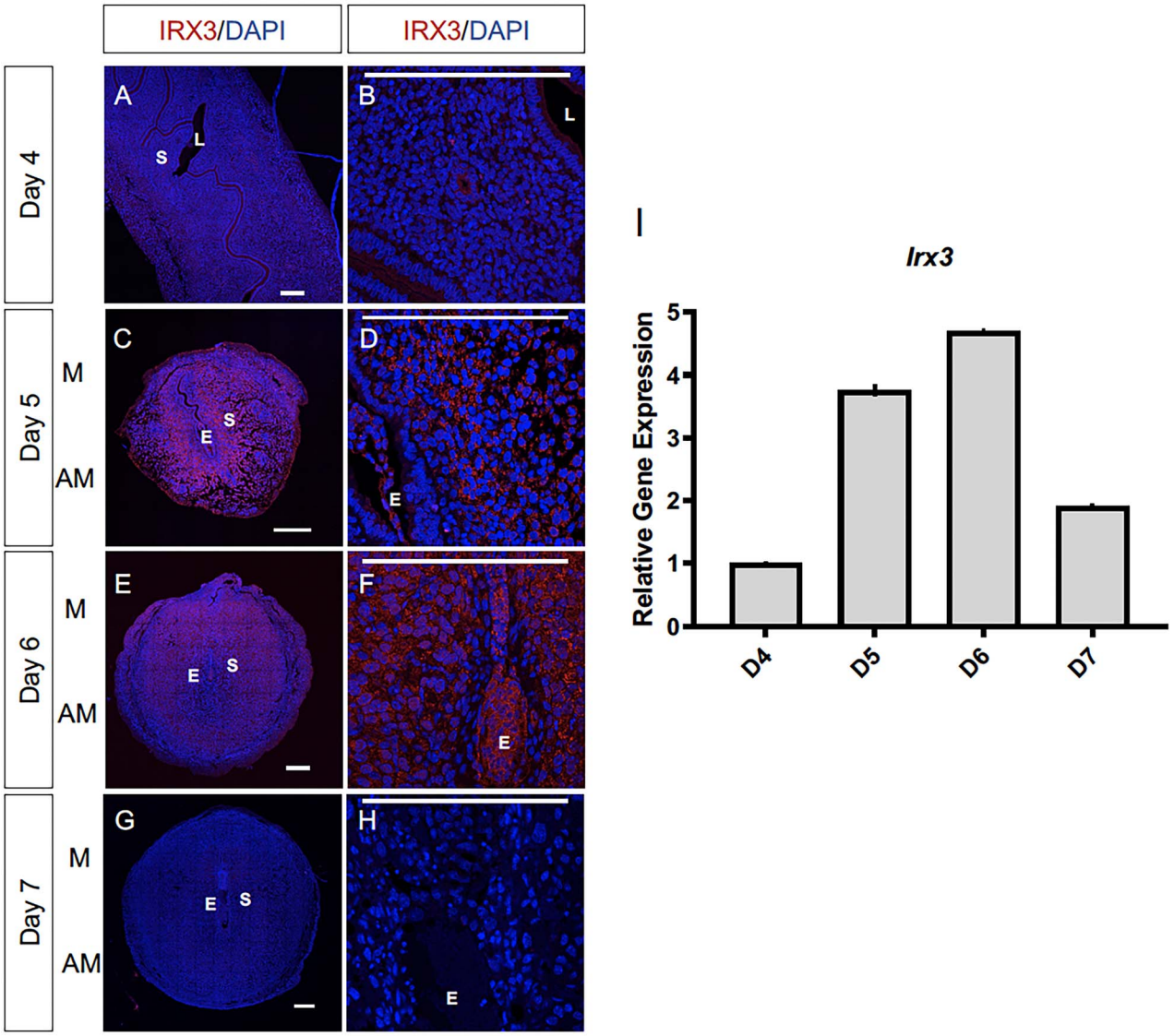

Figure 2. *Irx3* expression coincides with embryo implantation. (A–F) Immunofluorescence of IRX3 (red) co-labeled with DAPI, a nuclear marker (blue) throughout pregnancy days 4–7 (D4–D7) in wild type mice implantation sites ($n = 3$). Scale bars represent 250 μm. L: lumen; S: stroma; E: embryo; M: mesometrial; AM: anti-mesometrial. (I) Characterization of *Irx3* transcripts in the WT pregnant mouse uterus at D4-7. Real-time qPCR was determined by setting the expression level of *Irx3* mRNA on D4 of pregnancy to 1.0. Results are reported relative to 36b4 ($n = 3$). Data represent the mean ± SEM of three biological replicates performed in triplicate at each time point.

Antibody and primer authentication/validation

All antibodies were purchased from a commercial source. Antibody selections were made based on specificity as demonstrated by manufacturers that included a single band at the appropriate size on Western blot from positive control tissues and from cell lines transfected with factor-specific expression plasmids. Each antibody, except IRX3 (Invitrogen) is extensively referenced; we included references specific to their use as a decidualization marker in Supplementary Table S1. In addition, each experiment included no primary antibody controls; images are available upon request. The IRX3 antibody has been further validated by Western blot to ensure a single band at the appropriate size and a lack of a band upon interrogation of lysates from $Irx3^{LacZ/LacZ}$ tissues.

Primer sequences were selected based on historical use and references are available by request. Each laboratory routinely validates specificity and sensitivity of PCR primers using knockout animal tissues when possible ($Irx3^{LacZ/LacZ}$) or by using plasmid DNA dose–response curves.

Statistics

Statistics between groups were carried out using a two-sample t-test. Results were considered statistically significant if P-values were ≤ 0.05.

Results

Irx3$^{LacZ/LacZ}$ females exhibit defects in uterine vascularization with a marked reduction in implanted embryos

Previously, we determined that $Irx3^{LacZ/LacZ}$ females produced significantly fewer live pups over time compared to their controls, resulting in a subfertility phenotype. Ovarian histology and follicle counts identified oocyte deficits, but

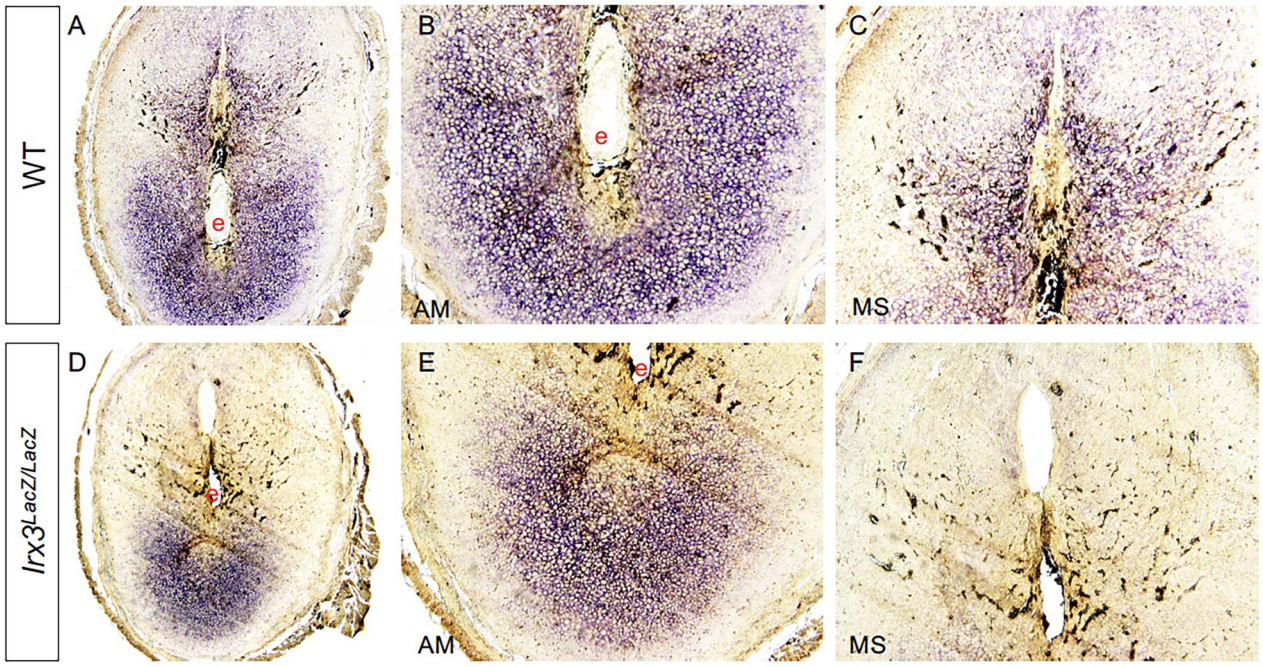

Figure 3. Alkaline phosphatase staining is diminished in *Irx3*$^{LacZ/LacZ}$ implantation sites. Day 7 uterine implantations sites from wild type (WT, A-C, $n=2$) and *Irx3*$^{LacZ/LacZ}$ (D–F, $n=2$) females were examined for alkaline phosphatase activity (purple stain). Magnified views of antimesometrial (AM) and mesometrial (MS) domains are shown adjacent to images of the entire implantation site. e: embryo

reproductive data suggested other factors were also contributing to the subfertility phenotype [13]. To understand the impact of *Irx3* on female fertility, we expanded our evaluation to examine uterine contributions of *Irx3* on fertility using *Irx3*$^{LacZ/LacZ}$ mice and their littermate controls over time. We investigated the integrity of implantation sites on D7 of pregnancy. Histological analysis of *Irx3*$^{LacZ/LacZ}$ (Figure 1B and D) and control (Figure 1A and C) implantation sites at D7 of gestation demonstrate that loss of *Irx3* impairs uterine vascularization, as depicted in the white boxes (Figure 1A–D). To investigate whether impaired implantation and defective vascularity were a result of hormonal deficiency, we measured circulating estrogen and progesterone (Figure 1E and F). Results showed that estrogen and progesterone levels were comparable between *Irx3*$^{LacZ/LacZ}$ and litter mate controls. To assess when the embryos were being lost in *Irx3*$^{LacZ/LacZ}$ females, we compared the number of implanted embryos to that of control mice on D7 and D11 of gestation (Figure 1G). By D7 we saw a significant decrease in the number of pups *in utero* in the *Irx3*$^{LacZ/LacZ}$ mice; however, there was no further reduction in pups between D7 and D11 indicating that pups were being lost at the onset of neoangiogenesis in the decidual bed during early pregnancy. Together these data demonstrate that *Irx3* has a role in female fertility with implications in uterine angiogenesis during embryo implantation.

Irx3 expression is confined to a discrete window during embryo implantation

Evidence of vascularity deficits within embryo implantation sites and early embryo loss suggested a role of *Irx3* in uterine implantation. Thus, we examined the protein and transcript profile of *Irx3* in the mouse uterus during normal pregnancy. Late on D4 of gestation, the mouse uterus is receptive and implantation ensues. At this time, IRX3 protein expression is detected predominately in the cytoplasm of the epithelial cells surrounding the lumen and uterine glands (Figure 2A and B). By D5, which is the onset of endometrial stromal cell decidualization, IRX3 protein expression is substantially increased, with expression expanding to the uterine stroma (S) immediately surrounding the embryo (E), also referred to as the primary decidual zone (Figure 2C and D). Similarly, at D6 of gestation, IRX3 expression is prominently expressed throughout the decidualized stroma, expanding further into the secondary decidual zone (Figure 2E and F). On D7 of gestation, nearing the end of the decidualization process, IRX3 protein expression is diminished (Figure 2G and H). Analysis of *Irx3* transcripts demonstrates a complimentary profile with expression initially documented at D4, followed by substantial increases at the onset of decidualization at D5 and D6 and a sharp decline toward the end of decidualization on D7. These data demonstrate that *Irx3* is induced in endometrial stromal cells at the onset of embryo implantation, the expression peaks during decidualization, and declines with the cessation of decidual phase of pregnancy.

Endometrial stromal cell differentiation is impaired in *Irx3*$^{LacZ/LacZ}$ females

The close spatio-temporal relationship between *Irx3* expression and the progression of decidualization led us to hypothesize that *Irx3* may play a role in this process. We, therefore, evaluated the expression of known regulators of decidualization in *Irx3*$^{LacZ/LacZ}$ and control uteri.

We analyzed the decidual response in *Irx3*$^{LacZ/LacZ}$ uteri by monitoring the expression of alkaline phosphatase (ALPL), a well-known biochemical marker of decidualization. As

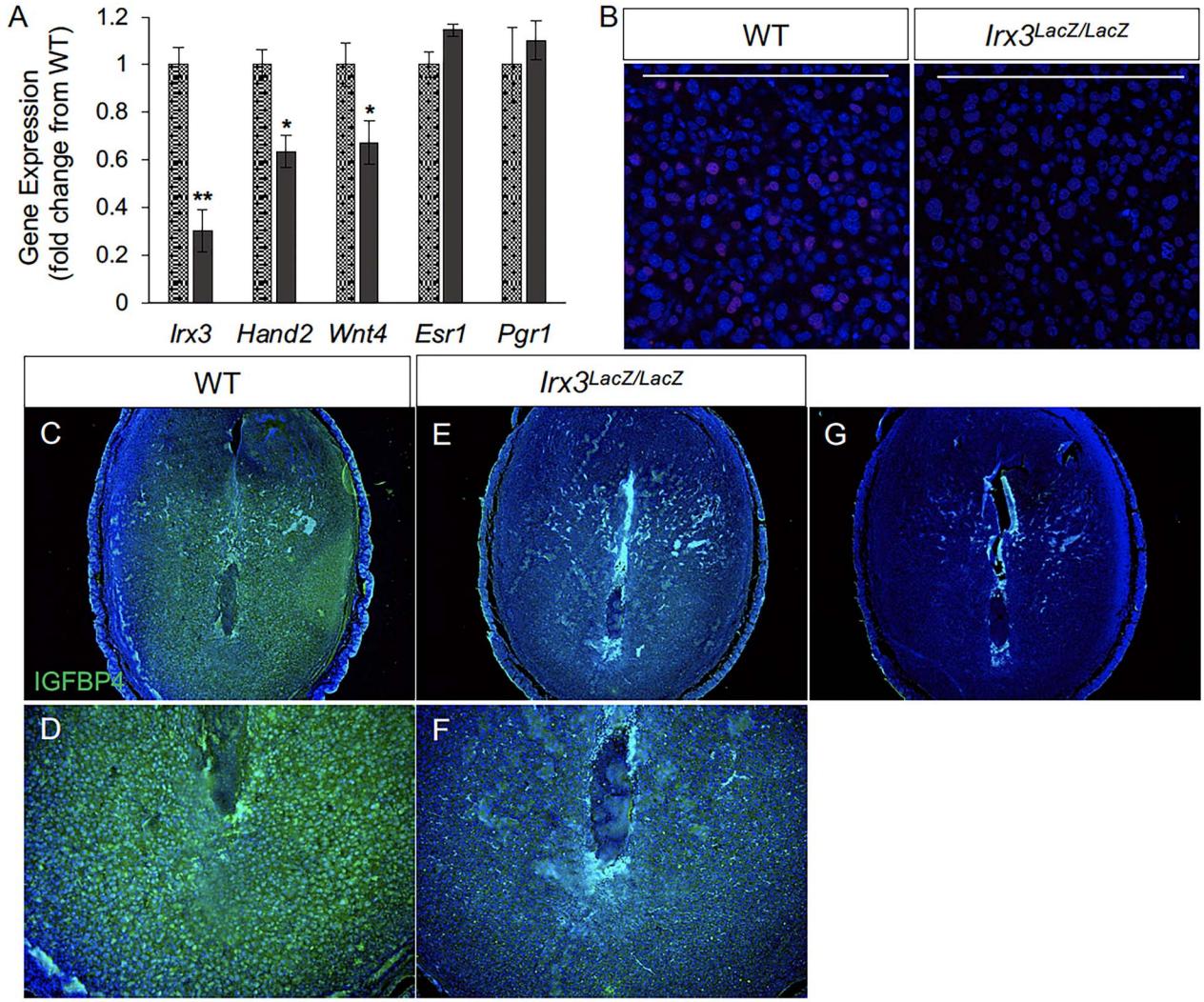

Figure 4. Decidualization is impaired in pregnant *Irx3*$^{LacZ/LacZ}$ uteri. (A) Real-time qPCR was performed using total RNA isolated from implantation sites from pregnant uteri of WT (stippled light gray) and *Irx3*$^{LacZ/LacZ}$ (dark gray) females on day 7 of pregnancy. Data represent the mean ± SEM of three biological replicates performed in triplicate at each time point. Fold change was calculated relative to transcript levels of the WT sample. Statistics: Student's *t*-test, $^{*}P < 0.05$. (B) Immunofluorescence of HAND2, a stromal cell marker (red) co-localized with DAPI, a nuclear marker (blue) at gestation D7 in control (WT, $n = 4$) and *Irx3*$^{LacZ/LacZ}$ ($n = 3$) implantation sites. Scale bars represent 250 mm. (C–F) Immunofluorescence of IGFBP4 (green, DAPI in blue), a marker for decidualized stromal cells at D7 in control (C, D) versus *Irx3*$^{LacZ/LacZ}$ (E, F) embryonic implantation sites. (D, F) Magnified views of the antimesometrial zone of the implantation sites for control (D) and *Irx3*$^{LacZ/LacZ}$ (F). (G) No antibody control.

expected, uterine sections from control mice exhibited prominent ALPL expression in both antimesometrial (AM) and mesometrial (M) areas on D7 of pregnancy (Figure 3A–C). In contrast, a strikingly reduced spatial expression of ALPL was seen in *Irx3*$^{LacZ/LacZ}$ uteri on D7 of pregnancy (Figure 3D–F). We further analyzed the decidualization response of *Irx3*$^{LacZ/LacZ}$ uteri by monitoring the expression of *Hand2* and *Wnt4*, factors that are induced in stromal cells during decidualization and play important regulatory roles during this process. As shown in Figure 4A, *Irx3* expression was already low in WT uteri at D7 (set to 1) and detectable, but extremely low (75–80% decreased) in the mutant decidua. Any transcripts present were likely derived from embryo tissue contamination. While steroid receptor genes *Esr1* and *Pgr1* remained unchanged, the expressions of *Wnt4* and *Hand2* were significantly decreased in mutant versus WT implantation sites. Further, HAND2 protein expression was weak and IGFBP4 was substantially reduced in *Irx3*$^{LacZ/LacZ}$ D7 stroma compared to WT as indicated by immunofluorescent analysis (Figure 4B–F), supporting qPCR results and suggesting defective decidualization.

It is important to address whether IRX3 controls stromal decidualization independent of embryonic development. We therefore subjected non-pregnant mice to experimentally induced decidualization in which a perturbation of the steroid-primed uteri triggers a decidual response in the absence of the implanting embryo. Uteri of ovariectomized WT and *Irx3*$^{LacZ/LacZ}$ mice were prepared by treating these animals with a well-established regimen of steroid hormones and the decidualization reaction was initiated by intraluminal injection of oil in one uterine horn while the other horn was left unstimulated. We then examined the gross anatomy of the stimulated and unstimulated uterine horns of WT and *Irx3*$^{LacZ/LacZ}$ mice. The uterine horns of WT mice exhibited a robust decidual response within 48 h after receiving the artificial stimulation (Figure 5A, left panel), whereas the

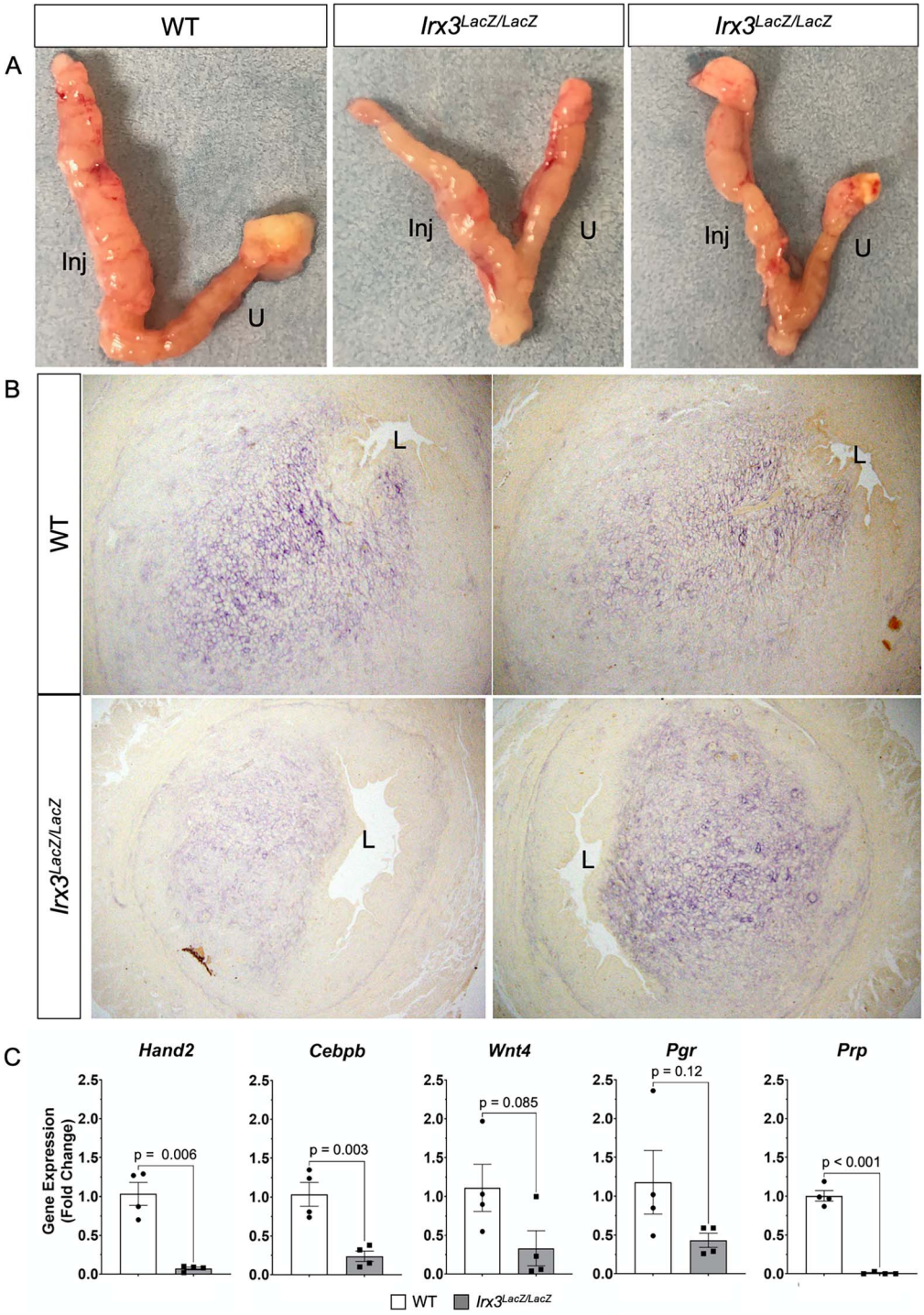

Figure 5. Artificial decidualization is impaired in *Irx3*$^{LacZ/LacZ}$ uteri. (A) Artificial decidualization was provoked by injection of oil into the left horn of each uterus (Inj); the right horn remained unstimulated (U). WT uteri (left panel, $n=3$) compared to *Irx3*$^{LacZ/LacZ}$ uteri (right panels, $n=2$), two examples. (B) Alkaline phosphatase staining from the stimulated horn in WT and *Irx3*$^{LacZ/LacZ}$ uteri, two examples of each. (C) Real-time qPCR of decidualization markers, *Hand2*, *Cebpb*, *Wnt4*, *Pgr*, and *Prp*, represented as the mean ± SE of the fold change from WT uteri, two samples taken from each horn. WT (white), *Irx3*$^{LacZ/LacZ}$ (gray).

Irx3$^{LacZ/LacZ}$ uteri showed a range of decidual responses, as expected based on their ability to carry some fetuses to term (Figure 5A, right panels). We next analyzed the decidualization responses of uteri by monitoring the expression of ALPL. In support of morphological results, some *Irx3*$^{LacZ/LacZ}$ uteri sections exhibited significantly reduced ALPL activity while others were comparable to the WT samples (Figure 5B). We further analyzed the decidualization response of *Irx3*$^{LacZ/LacZ}$ uteri by monitoring the expression of *Hand2*, *Prp*, *Cebpb*, *Pgr*, and *Wnt4*, factors that are induced in stromal cells during decidualization and play important regulatory roles during this process. As shown in Figure 5C, expression in response to artificial decidualization was decreased in *Irx3*$^{LacZ/LacZ}$ uteri with significant downregulation of mRNAs corresponding to

Hand2, *Prp* and *Cebpb* along with a trend to significance in decreased expression for *Wnt4* and *Pgr*. Variability of expression levels from individual replicates are representative of variable outcomes in pregnancy.

Compromised neoangiogenesis in the decidual bed of *Irx3* KO females

To further evaluate the vascularization defect found in $Irx3^{LacZ/LacZ}$ implantation sites, we examined whether loss of *Irx3* expression affected angiogenesis. Thus, we analyzed the angiogenic response in $Irx3^{LacZ/LacZ}$ uteri by monitoring an endothelial cell marker, CD31 (platelet endothelial cell adhesion molecule-1, PECAM-1), at D7 of gestation (Figure 6A–G). As expected, implantation sites from control mice exhibited prominent CD31 expression in both the antimesometrial (AM) and mesometrial (M) areas on D7 of pregnancy (Figure 6A, C and E). In contrast, while expression of CD31 in $Irx3^{LacZ/LacZ}$ implantation sites was not different in the mesometrial side (Figure 6D and G), quantification of expression showed a significant decrease of CD31 expression in the antimesometrial region (Figure 6B, F and G). These results supported the concept that the loss of *Irx3* expression in the stroma is responsible for the reduction in the endothelial cell population in the antimesometrial decidua.

The lack of endothelial cell proliferation in $Irx3^{LacZ/LacZ}$ uteri was further ascertained by immunostaining for Ki67, a marker for cell proliferation (Figure 7). While the uterine sections obtained from WT mice on D7 of pregnancy exhibited robust Ki67 immunostaining in endothelial cells, consistent with microvascular proliferation, those obtained from mutant animals showed greatly reduced Ki67 staining, confirming compromised endothelial cell proliferation in the absence of stromal *Irx3* expression.

Fewer and unorganized gap junction connections in $Irx3^{LacZ/LacZ}$ uteri

To gain further insights on the impact of *Irx3* loss on vascularization, we investigated GJA1, a gap junction protein critical in modulating stromal differentiation and neovascularization during murine implantation [15]. In our previous investigations, $Irx3^{LacZ/LacZ}$ ovaries demonstrated no change in *Gja1* transcripts between mutant and control, but they detected abnormal deposition of GJA1, which resulted in follicle death [13]. Based on these data, we tested whether loss of *Irx3* in the uterus would impair GJA1 expression during embryo implantation. Complementary to our ovarian expression data, we found that loss of *Irx3* resulted in no change in *Gja1* transcripts (Figure 8A), but significantly disrupted GJA1 protein localization in both mesometrial and anti-mesometrial regions of the uterine stroma (Figure 8B–J). Together these data suggest that *Irx3* functions to promote embryo implantation through appropriate cell–cell communication to provide the proper environment for successful decidualization and neovascularization.

Discussion

The Iroquois genes have been implicated in embryonic patterning and can be found in a range of tissues, with roles in organization of the spinal cord, limb, bone, and heart, to name a few [12, 16–18]. Previously, we identified IRX3 and IRX5 expression in mouse ovaries, but not testes, starting

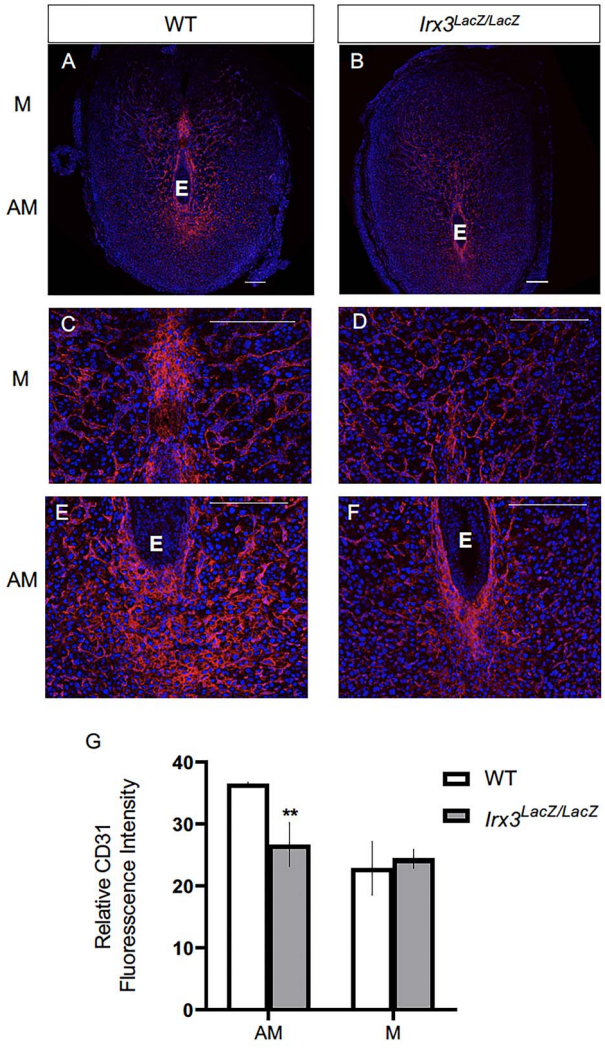

Figure 6. $Irx3^{LacZ/LacZ}$ uteri exhibit impaired vascularization by day 7 of gestation. (A–F) Immunofluorescence of endothelial cell marker, CD31 (CD31/PECAM, red) co-labeled with DAPI, a nuclear marker (blue) at pregnancy D7 in control (A, C, E, $n=3$) and $Irx3^{LacZ/LacZ}$ (B, D, F, $n=3$) implantation sites. Scale bars represent 250 mm. E: embryo; M: mesometrial; AM: anti-mesometrial. (G) Quantification of relative CD31 fluorescence intensity in the anti-mesometrium (AM) and mesometrium (M). Data represent mean ± SEM. Statistics: two-sample *t*-test; **: $P < 0.01$.

after sex determination [19]. This led to a series of investigations to discern the role of IRX3 and IRX5 in the ovary during development. Using mutant mice lacking both *Irx3* and *Irx5*, we discovered mutant ovaries had abnormal granulosa cell morphology and disturbed granulosa cell–oocyte interactions [13]. A closer look at ablation of *Irx3* alone, using $Irx3^{LacZ/LacZ}$ mutant females, indicated that loss of *Irx3* caused reduced follicle numbers; however, this did not fully explain the profound deficit in fertility as indicated by at least 50% loss in live pup births compared to WT females [20]. This prompted us to investigate whether IRX3 was affecting embryo implantation. Results from the current study suggest multifaceted roles for IRX3 in female fertility that include important functions in both ovary and pregnant uterus. In particular, we report that IRX3 functions in early pregnancy to establish successful embryo–uterine interactions.

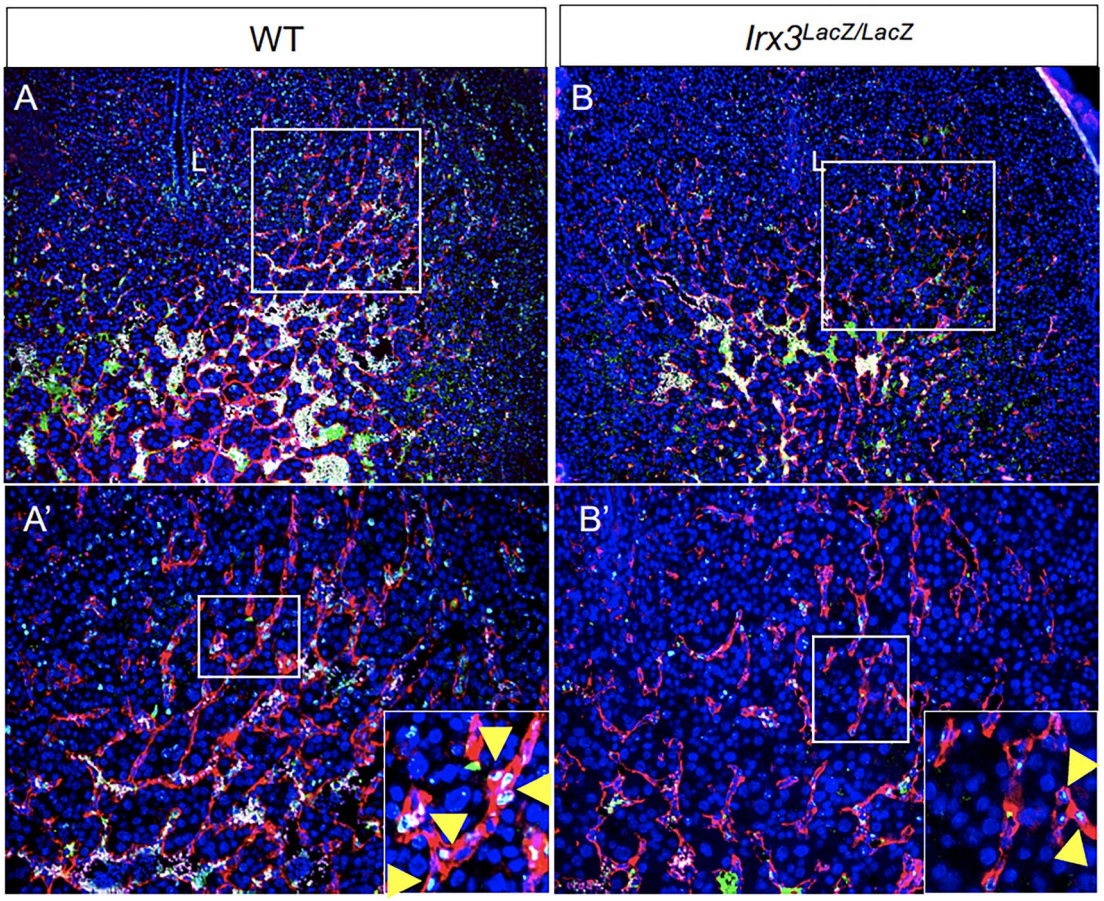

Figure 7. Fewer endothelial cells proliferate in *Irx3*$^{LacZ/LacZ}$ implantation sites. (A, B) Endothelial cell proliferation within implantation sites was evaluated using immunofluorescence co-staining for proliferation marker, Ki67 (green), and endothelial cell marker, CD31/PECAM (red) (DAPI, nuclear stain, blue) in wild type (A) vs *Irx3*$^{LacZ/LacZ}$ (B) uteri. Boxes in A–B are shown at higher magnification in A′-B′; L: uterine lumen. Boxes in A′-B′ are shown at higher magnification in insets. Yellow arrowheads indicate examples of Ki67 stain within endothelial cells.

These data provide a foundation for new discoveries of how IRX3 functions in a spatiotemporal manner in the uterus to promote successful embryo–uterine interactions via establishment of proper cell–cell communications to support both decidualization and angiogenesis.

Establishment of a robust and healthy vascular network is essential for reproduction as it supports folliculogenesis, ovarian hormone production, ovulation, implantation, and embryonic growth [21–23]. Evaluation of the integrity of *Irx3*$^{LacZ/LacZ}$ implantation sites on D7 revealed reduced vascularity with a concomitant decline in the number of implanted embryos, indicating disruptions in reproductive fecundity in *Irx3*$^{LacZ/LacZ}$ mice. Together these data demonstrate that *Irx3* has a role in uterine angiogenesis during embryo implantation.

In the murine model, implantation begins late on D4 when the mouse uterus is receptive to implantation [24]. At D5, the decidualization process begins and the stromal cells of the uterus differentiate into a unique secretory tissue, the decidua. The stromal cells immediately surrounding the embryo are transformed into the primary decidual cells and further expand into the secondary decidual cells until the invasive period is complete [9]. Here, we demonstrate that the expression profile of IRX3 in uterine stromal cells is intimately associated with the decidualization phase of mouse pregnancy. Notably, during the mid-secretory phase of the human menstrual cycle, studies show that *IRX3* expression increases as the uterus becomes receptive to implantation [25–27]. Contrary to mice, the human uterus begins decidualizing in the nonpregnant state, during the mid-secretory phase with an expansion of decidualization once the pregnancy is established [28]. Taken together, these data and our studies have uncovered a conserved physiological timing of *Irx3* expression in the human and murine uterus that corresponds to the onset of decidualization in both species.

As decidualization progresses, the uterus undergoes expansive tissue remodeling, critical for proper maternal–fetal interactions. Following the attachment of the blastocyst to the uterine epithelium, the underlying stromal cells differentiate into decidual cells with unique biosynthetic and secretory profiles needed to promote this transformation. We found that IRX3 is robustly induced in the decidual tissue during a critical time frame in mouse implantation and angiogenesis. Factors secreted by the decidualizing stromal cells promote tissue and vascular remodeling; thus, it is conceivable that IRX3, produced by the decidualizing stromal cells, has a role in preparing the uterus for appropriate embryo–uterine interactions. We recognize the importance of teasing out oocyte/embryo versus uterine stromal cell roles of IRX3; future studies will be undertaken to evaluate implantation success by D5 in addition to embryo transfer experiments between WT and *Irx3*$^{LacZ/LacZ}$ females. Herein, however, we report an impaired

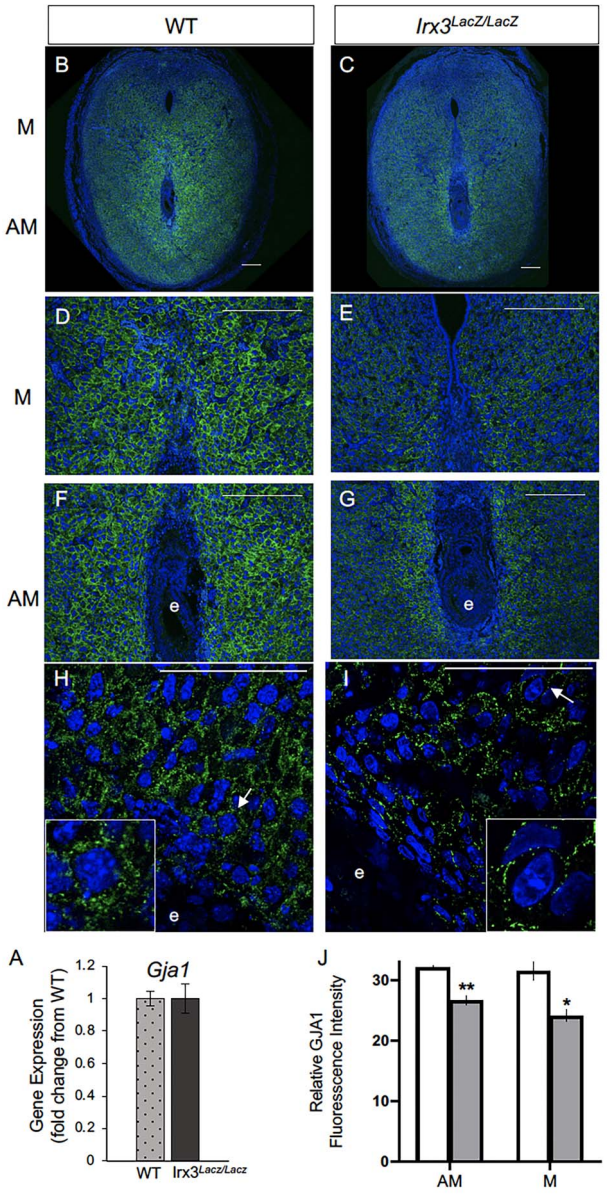

Figure 8. *Irx3*$^{LacZ/LacZ}$ uteri express similar *Gja1* transcripts but abnormal GJA1 protein. (A) Real-time qPCR results for *Gja1* from pregnant uteri of WT and *Irx3*$^{LacZ/LacZ}$ females on D7 of pregnancy. Data represent the mean ± SEM of three biological replicates performed in triplicate at each time point. Fold change was calculated relative to transcript levels of the WT sample. Statistics: Student's *t*-test, $^{*}P < 0.05$. (B–I) Immunofluorescence of gap junction protein 1 (GJA1, connexin 43, green) co-labeled with DAPI, a nuclear marker (blue) at gestation D7 in control (B, D, F, H, $n = 4$) and *Irx3*$^{LacZ/LacZ}$ (C, E, G, I, $n = 5$) implantation sites. Images are represented in increasing magnification, scale bars represent 250 mm. Arrows highlight single cells that are enlarged within the inset of H and I. (J) Quantification of relative GJA1 fluorescence intensity in the anti-mesometrium (AM, $P = 0.01$) and mesometrium (M, $P = 0.027$) in wild type (white bars) vs *Irx3*$^{LacZ/LacZ}$ females (light gray bars). Data represent mean ± SEM. Statistics: two-sample *t*-test, *: $P < 0.05$; **: $P < 0.01$.

decidual response in *Irx3*$^{LacZ/LacZ}$ uteri by D7 of standard pregnancy, as well as by artificial decidual reaction. Marked reduction in expression of biomarkers of stromal differentiation was observed in both strategies. It has been suggested that stromal differentiation and angiogenesis are intimately connected processes during pregnancy [15]. Along with a difference in the presence of a subset of decidualization markers, we also observed a substantial decrease in CD31 expression, an endothelial cell marker, in the *Irx3*$^{LacZ/LacZ}$ implantation sites. Collectively, the reduction in vascularization seen at D7 by both histological analysis and immunohistochemistry, demonstrates that ablation of *Irx3* leads to improper vascularization in the mouse uterus during early pregnancy. This defect in vascularization in *Irx3*$^{LacZ/LacZ}$ uteri was due to compromised endothelial cell proliferation. Uterine natural killer cells, which are implicated in vascular remodeling, were similar in WT and *Irx3*$^{LacZ/LacZ}$ mice (Supplementary Figure S1).

Previously, we identified that loss of both *Irx3* and *Irx5* impaired gap junction protein deposition in ovarian follicles, leading to follicle and oocyte death [13]. Here, we discovered a potentially conserved role for *Irx3* in mediating proper cell–cell communication via gap junction expression during embryo implantation. Early studies identified three connexins in the human uterus: connexin 26, connexin 32, and connexin 43 [29]. Of these, connexin 43 (GJA1) is the predominant subtype expressed in human and mouse endometrium and localized almost exclusively to the stroma, connecting decidual cells [30]. Conditional knockout of *Gja1* in the mouse uterus resulted in severe subfertility with aberrant differentiation of the uterine stroma and significant reduction in VEGF [15]. Further, maternal decidua isolated from women with recurrent early pregnancy loss was found to have reduced *Gja1* transcripts and protein when compared with controls [31]. The importance of GJA1 regulation during pregnancy is augmented by epidemiological studies that identified taking mefloquine, an anti-malarial compound that blocks GJA1, as a risk factor for spontaneous abortion [32]. Here, our data indicate that IRX3 is instrumental in mediating proper cell–cell communication via GJA1 expression. In the uterus and ovary, GJA1 serves a critical role in establishing communications between cells, promoting both oocyte competence in the ovary and angiogenesis in the uterus during pregnancy [15, 33, 34]. Our results indicate that IRX3 promotes successful cell–cell connections allowing for appropriate intercellular cross talk throughout the intimate correspondence of embryo implantation and angiogenesis during pregnancy.

Embryo implantation is achieved when a competent oocyte develops into a blastocyst capable of facilitating embryo–uterine interactions with the receptive endometrium. It is clear that IRX3 has a significant role in mouse reproductive health including oocyte competence and endometrial angiogenesis [15, 33, 34]. Impaired uterine receptivity and poor vascularization are major causes of early pregnancy loss. Therefore, understanding how *Irx3* is regulated during this critical window of implantation may provide insights and solutions for female reproductive health and fertility.

Supplementary material

Supplementary material is available at *BIOLRE* online.

Acknowledgments

We thank all members of the Jorgensen laboratory for comments and support. We also thank Emily Huber and Eowyn Liu for their help with sectioning. We truly appreciate all of the comments, advice, and technical support from the Developmental Endocrinology Group at the University of Wisconsin–Madison School of Veterinary Medicine. We are immensely grateful for Miranda Sun and Daniel Radecki for their

support in microscopy trainings and Image J. We would also like to show our gratitude to Annie Novak and Tori Gronemeyer for their exemplary mouse husbandry work.

Data availability

The data underlying this article are available in the article and in its online supplementary material.

References

1. Kim SM, Kim JS. A review of mechanisms of implantation. *Dev Reprod* 2017; **21**:351–359.
2. Psychoyos A. Implantation. In: Greep RO, Astwood EG, Geiger SR (eds.), *Handbook of Physiology*. Washington DC: American Physiology Society; 1973: 187–215.
3. Yoshinaga K. Uterine receptivity for blastocyst implantation. *Ann N Y Acad Sci* 1988; **541**:424–431.
4. Parr MB, Parr EL. The implantation reaction. In: Wynn RM (ed.), *Biology of the Uterus*. New York: Plenum Press; 1989: 233–277.
5. Weitlauf HM. Biology of Implantation. In: Knobil E, Neill JD (eds.), *The Physiology of Reproduction*. New York: Raven Press Ltd.; 1994: 391–440.
6. Cross JC, Werb Z, Fisher SJ. Implantation and the placenta: key pieces of the development puzzle. *Science* 1994; **266**:1508–1518.
7. Giudice LC, Irwin JC. Roles of the insulinlike growth factor family in nonpregnant human endometrium and at the decidual: trophoblast interface. *Semin Reprod Endocrinol* 1999; **17**:13–21.
8. Carson DD, Bagchi I, Dey SK, Enders AC, Fazleabas AT, Lessey BA, Yoshinaga K. Embryo implantation. *Dev Biol* 2000; **223**:217–237.
9. Ramathal CY, Bagchi IC, Taylor RN, Bagchi MK. Endometrial decidualization: of mice and men. *Semin Reprod Med* 2010; **28**: 17–26.
10. Gomez E, Ruiz-Alonso M, Miravet J, Simon C. Human endometrial transcriptomics: implications for embryonic implantation. *Cold Spring Harb Perspect Med* 2015; **5**:a022996.
11. Bosse A, Stoykova A, Nieselt-Struwe K, Chowdhury K, Copeland NG, Jenkins NA, Gruss P. Identification of a novel mouse Iroquois homeobox gene, Irx5, and chromosomal localisation of all members of the mouse Iroquois gene family. *Dev Dyn* 2000; **218**: 160–174.
12. Peters T, Dildrop R, Ausmeier K, Ruther U. Organization of mouse Iroquois homeobox genes in two clusters suggests a conserved regulation and function in vertebrate development. *Genome Res* 2000; **10**:1453–1462.
13. Fu A, Oberholtzer SM, Bagheri-Fam S, Rastetter RH, Holdreith C, Caceres VL, John SV, Shaw SA, Krentz KJ, Zhang X, Hui CC, Wilhelm D *et al.* Dynamic expression patterns of Irx3 and Irx5 during germline nest breakdown and primordial follicle formation promote follicle survival in mouse ovaries. *PLoS Genet* 2018; **14**:e1007488.
14. Zhang SS, Kim KH, Rosen A, Smyth JW, Sakuma R, Delgado-Olguin P, Davis M, Chi NC, Puviindran V, Gaborit N, Sukonnik T, Wylie JN *et al.* Iroquois homeobox gene 3 establishes fast conduction in the cardiac His-Purkinje network. *Proc Natl Acad Sci U S A* 2011; **108**:13576–13581.
15. Laws MJ, Taylor RN, Sidell N, DeMayo FJ, Lydon JP, Gutstein DE, Bagchi MK, Bagchi IC. Gap junction communication between uterine stromal cells plays a critical role in pregnancy-associated neovascularization and embryo survival. *Development* 2008; **135**: 2659–2668.
16. Cavodeassi F, Modolell J, Gomez-Skarmeta JL. The Iroquois family of genes: from body building to neural patterning. *Development* 2001; **128**:2847–2855.
17. Gomez-Skarmeta JL, Modolell J. Iroquois genes: genomic organization and function in vertebrate neural development. *Curr Opin Genet Dev* 2002; **12**:403–408.
18. Houweling AC, Dildrop R, Peters T, Mummenhoff J, Moorman AF, Ruther U, Christoffels VM. Gene and cluster-specific expression of the Iroquois family members during mouse development. *Mech Dev* 2001; **107**:169–174.
19. Jorgensen JS, Gao L. Irx3 is differentially up-regulated in female gonads during sex determination. *Gene Expr Patterns* 2005; **5**: 756–762.
20. Fu A, Koth ML, Brown RM, Shaw SA, Wang L, Krentz KJ, Zhang X, Hui CC, Jorgensen JS. IRX3 and IRX5 collaborate during ovary development and follicle formation to establish responsive granulosa cells in the adult mouse†. *Biol Reprod* 2020; **103**: 620–629.
21. Jiang JY, Macchiarelli G, Tsang BK, Sato E. Capillary angiogenesis and degeneration in bovine ovarian antral follicles. *Reproduction* 2003; **125**:211–223.
22. Yamada O, Abe M, Takhana K, Iwasa K, Hiraga T, Hiratsuka T. Microvasculature of mature bovine follicles and its changes with ovulation. *J Reprod Dev* 1994; **40**:307–315.
23. Ferrara N, Carver-Moore K, Chen H, Dowd M, Lu L, O'Shea KS, Powell-Braxton L, Hillan KJ, Moore MW. Heterozygous embryonic lethality induced by targeted inactivation of the VEGF gene. *Nature* 1996; **380**:439–442.
24. Paria BC, Huet-Hudson YM, Dey SK. Blastocyst's state of activity determines the "window" of implantation in the receptive mouse uterus. *Proc Natl Acad Sci U S A* 1993; **90**:10159–10162.
25. Tseng LH, Chen I, Chen MY, Yan H, Wang CN, Lee CL. Genome-based expression profiling as a single standardized microarray platform for the diagnosis of endometrial disorder: an array of 126-gene model. *Fertil Steril* 2010; **94**:114–119.
26. Zhang D, Sun C, Ma C, Dai H, Zhang W. Data mining of spatial-temporal expression of genes in the human endometrium during the window of implantation. *Reprod Sci* 2012; **19**:1085–1098.
27. Chan C, Virtanen C, Winegarden NA, Colgan TJ, Brown TJ, Greenblatt EM. Discovery of biomarkers of endometrial receptivity through a minimally invasive approach: a validation study with implications for assisted reproduction. *Fertil Steril* 2013; **100**: 810–817.
28. Gellersen B, Brosens IA, Brosens JJ. Decidualization of the human endometrium: mechanisms, functions, and clinical perspectives. *Semin Reprod Med* 2007; **25**:445–453.
29. Jahn E, Classen-Linke I, Kusche M, Beier HM, Traub O, Grummer R, Winterhager E. Expression of gap junction connexins in the human endometrium throughout the menstrual cycle. *Hum Reprod* 1995; **10**:2666–2670.
30. Yu J, Berga SL, Zou W, Yook DG, Pan JC, Andrade AA, Zhao L, Sidell N, Bagchi IC, Bagchi MK, Taylor RN. IL-1beta inhibits connexin 43 and disrupts decidualization of human endometrial stromal cells through ERK1/2 and p38 MAP kinase. *Endocrinology* 2017; **158**:4270–4285.
31. Nair RR, Jain M, Singh K. Reduced expression of gap junction gene connexin 43 in recurrent early pregnancy loss patients. *Placenta* 2011; **32**:619–621.
32. Nevin RL. Mefloquine blockade of connexin 43 (Cx43) and risk of pregnancy loss. *Placenta* 2011; **32**:712.
33. Ackert CL, Gittens JE, O'Brien MJ, Eppig JJ, Kidder GM. Intercellular communication via connexin43 gap junctions is required for ovarian folliculogenesis in the mouse. *Dev Biol* 2001; **233**: 258–270.
34. Winterhager E, Kidder GM. Gap junction connexins in female reproductive organs: implications for women's reproductive health. *Hum Reprod Update* 2015; **21**:340–352.